Performances of High Numerical Aperture Water and Oil Immersion Objective in Deep-Tissue, Multi-Photon Microscopic Imaging of Excised Human Skin

CHEN-YUAN DONG,[1] BETTY YU,[2] PETER D. KAPLAN,[3] AND PETER T.C. SO[4]*
[1]*Department of Physics, National Taiwan University, Taipei 106, Taiwan, R.O.C.*
[2]*Department of Chemical Engineering, Massachusetts Institute of Technology, Cambridge, Massachusetts 02139*
[3]*Univerlever Edgewater Laboratory, Edgewater, New Jersey 07020*
[4]*Department of Mechanical Engineering, Massachusetts Institute of Technology, Cambridge, Massachusetts 02139*

KEY WORDS multi-photon; skin, deep-tissue; fluorescence; microscopy

ABSTRACT Multi-photon fluorescence microscopy (MPFM) is a powerful technique for imaging scattering, biological specimens in depth. In addition to the sectioning effect generated by the point-like excitation volume, the near-infrared wavelengths used for multi-photon excitation allow deeper penetration into optically turbid specimens. In physiological specimens, the optical properties such as the scattering coefficients and refractive indices are often heterogeneous. In these specimens, it is not clear which type of immersion objective can provide optimized images in-depth. In particular, in-depth dermatological imaging applications using MPFM requires such optimization to obtain qualitative and quantitative information from the skin specimens. In this work, we address this issue by comparing the performances of two common types of high numerical aperture (NA) objectives: water-immersion and oil-immersion. A high-quality water-immersion objective (Zeiss, 40× C-Apochromat, NA 1.2) and a comparable oil-immersion objective (Zeiss, 40× Fluar, NA 1.25) were used for in-depth imaging of autofuorescent excised human skin and sulforhodamine B treated human skin specimens. Our results show that in the epidermal layers, the two types of immersion objectives perform comparably. However, in the dermis, multi-photon imaging using the oil immersion objective results in stronger fluorescence detection. These observations are most likely due to the degraded point-spread-function (PSF) caused by refractive index mismatch between the epidermis and the dermis. *Microsc. Res. Tech. 63:81–86, 2004.*

INTRODUCTION

The experimental introduction of two-photon microscopy by Webb's group in Cornell University (Denk et al., 1990) represents an important milestone in the development of modern optical microscopy. In this technique, a UV or visible excitable fluorescent molecule undergoes transition to the excited state by the simultaneous absorption of two near-infrared photons. Compared to commonly used one-photon excitation techniques, two-photon fluorescence microscopy offers a number of distinct advantages. First, since the high photon flux required for non-linear excitation limits sample excitation to near the focus of an objective, imaging with a confined, sub-femtoliter spot results in strong axial depth discrimination and reduced photodamage. In addition, two-photon microscopy has the unique capability to image optically turbid specimens at great depths, non-invasively. Compared to the ultraviolet (UV) or visible photons, the near-infrared light source used for two-photon excitation is absorbed and scattered less by tissues. The improved penetration depth allows in-depth, three-dimensional examination of biological specimens (Centonze and White, 1998; So et al., 2000). For biological and biomedical applications, two-photon microscopy has demonstrated its capabilities in neurobiology (Svoboda et al., 1997; Yuste and Denk, 1995) and embryology (Squirrell et al., 1999). In other tissue structures such as the cornea and skin, two-photon microscopy has been successfully applied for minimally-invasive, deep-tissue imaging (Masters et al., 1997; Piston et al., 1995). Specifically, two-photon microscopy has tremendous applications in dermatology. In addition to providing 3-D morphological information of skin under ex vivo or in vivo conditions, two-photon microscopy has also been recently applied to investigating transdermal transport pathways of hydrophilic and hydrophobic molecules under chemical enhancer actions (Yu et al., 2001, 2002). These studies reveal the microscopic details of molecular transport and offer insights into improving drug delivery methodology. In-depth, multi-photon examination of biological specimen is now commonplace. We routinely image human skin up to the depths on the order of 100 μm, often reaching the limits in working distances of many high numerical aperture, oil-immersion objectives.

SPHERICAL ABERRATION AND WATER AND OIL-IMMERSION OBJECTIVES IN MULTI-PHOTON IMAGING

In imaging biological specimens, conventional wisdom dictates the use of water immersion microscope

*Correspondence to: Peter T.C. So, Department of Mechanical Engineering, Massachusetts Institute of Technology, 77 Massachusetts Avenue, Cambridge, MA 02139. E-mail: ptso@mit.edu

Received 11 September 2003; accepted in revised form 15 September 2003
DOI 10.1002/jemt.10431
Published online in Wiley InterScience (www.interscience.wiley.com).

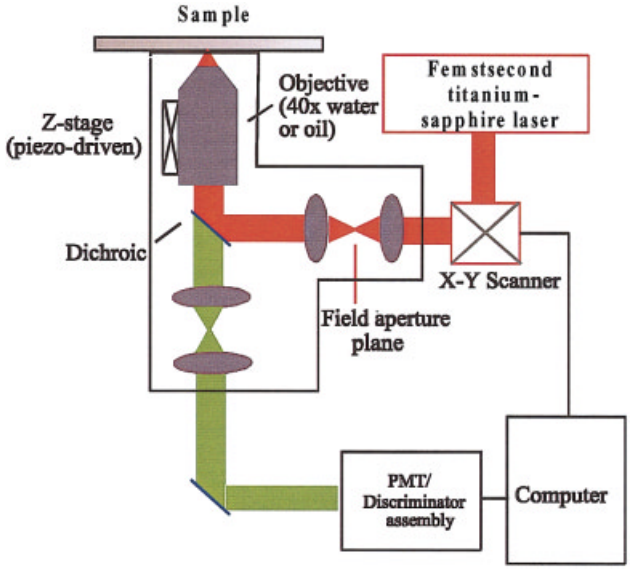

Fig. 1. A two-photon fluorescence microscope. [Color figure can be viewed in the online issue, which is available at www.interscience.wiley.com.]

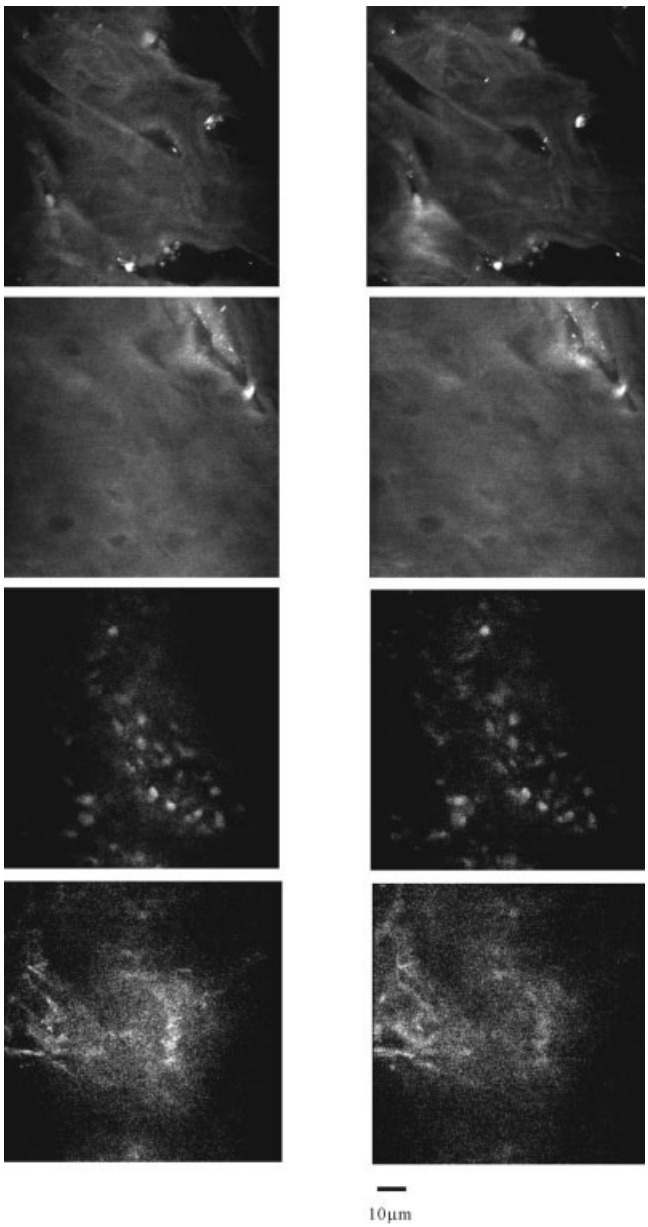

Fig. 2. Multiphoton excited auto-fluorescent images of the skin at different layers. Representative images from the stratum corneum, deeper epidermal layer, basal layer, and upper dermis (top to bottom) acquired using a water (left row) and oil (right row) immersion objective are shown.

objectives. The logic behind this choice is due to the fact that biological specimens examined by optical microscopy are often immersed cellular monolayers cultured on flat, optical surfaces. The aqueous environment of the cells' surrounding and interior means that the refractive index of the specimens is very close to 1.33, water's index of refraction. Therefore, in these specimens, optical imaging performed with water immersion objectives minimizes image distortion due to refractive index difference induced spherical aberration. While this argument is sound for 3-D cellular systems such as tissue-engineered constructs, it is not valid for all biological specimens. In particular, for dermatological imaging, the choice of immersion objectives is complicated by the rapidly varying refractive indices of typical skin specimens.

For example, it has been shown that the refractive index varies significantly within different layers of the skin. From optical coherence tomography (OCT) studies, a detailed map of the refractive index was obtained from the epidermis into the upper dermal layer. To be specific, the index of refraction in the stratum corneum was found to be 1.47, a value close to that of glass. At greater depths, the refractive index decreases to 1.43 in the granular layer and 1.34 in the basal layer. Below the epidermal layers, the refractive index rises back to about 1.41 in the upper dermis (Halliday et al., 1992; Knüttel and Boehlau-Godau, 2000; Tearney et al., 1995). Compared with the refractive indices of some transparent media, the skin surface is glass-like and the basal layer is water-like while the index of refraction in the upper dermis lies in between (Halliday et al., 1992). In addition to refractive index changes, sample scattering coefficients can also adversely affect imaging characteristics. Like the refractive index, the scattering coefficient within the skin also varies as a function of depth. To be specific, OCT studies described above revealed that the scattering coefficient within the stratum corneum is around 1–1.5 mm^{-1}. In deeper epidermal layers, the coefficients increased to 6–7 mm^{-1} in the granular layer and their values change to 4–5 mm^{-1} in the basal layer. Beyond the epidermis, the scattering coefficient slightly increases to around 5–8 mm^{-1} in the upper dermis (Tearney et al., 1995; Knüttel and Boehlau-Godau, 2000).

Therefore, to optimize imaging quality for in-depth, multi-photon imaging of skin, one needs to separate the effects of refractive index mismatch and scattering

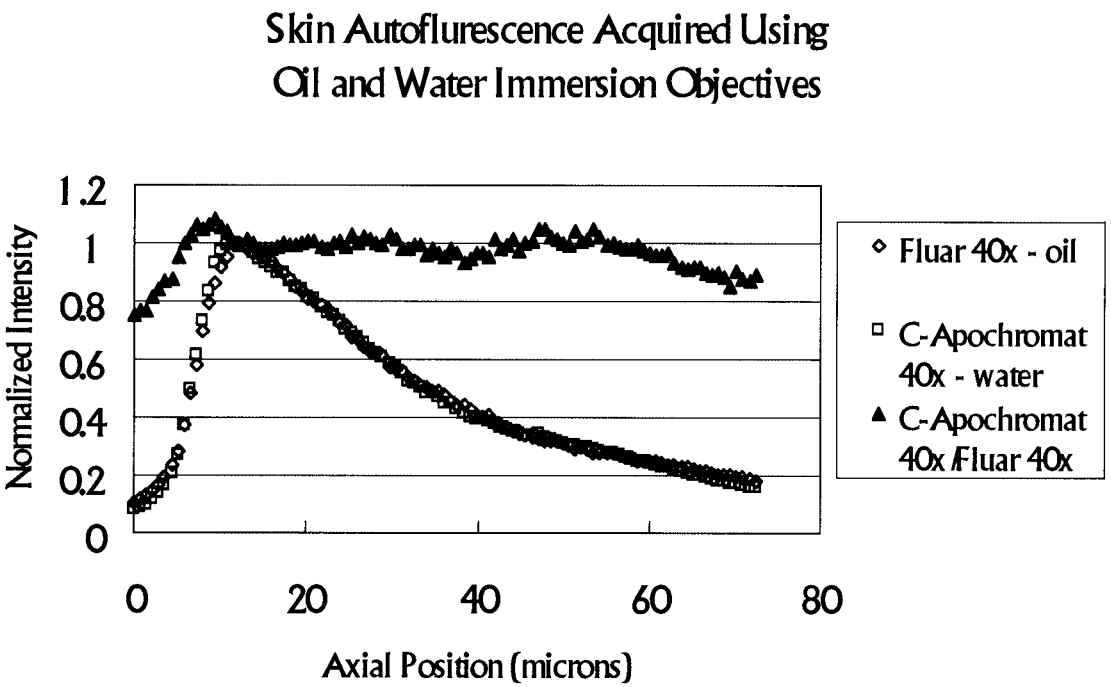

Fig. 3. Skin autofluorescence axial profiles (with fluorescence ratio) acquired with the water and oil immersion objectives.

on skin imaging. Previous studies showed that the range of scattering coefficients in skin has minimum effects on the PSF widths (Dong et al., 2003; Dunn et al., 2000). Therefore, it appears that scattering does not contribute to the degradation of image resolution in two-photon imaging of the epidermis and upper dermis. In fact, the refractive index mismatch induced degradation of lateral and axial resolution has been reported with confocal microscopy (Hell et al., 1993) and similar effects have been demonstrated with two-photon microscopy (de Gauw et al., 1999; Dong et al. 2003; Gerritsen and de Gauw, 1999). While it is difficult to characterize the combined effects of spherical aberration and scattering on multi-photon skin imaging, it is possible to focus on the effects of spherical aberration by comparing the skin images acquired using objectives of different immersion media. In this study, we chose to compare the skin imaged acquired using water and oil immersion objectives, two of the commonly used immersion objective types.

The two objectives chosen for this study are two high numerical aperture (NA) objectives: a water immersion objective (Zeiss, 40× C-Apochromat, NA 1.2) and an oil lens (Zeiss, 40× Fluar, NA 1.25). While they should perform comparably at the skin surface, it is not clear how the skin's complex refractive index profiles change image quality and detected fluorescence at greater depths. There are a number of reasons why the water and oil immersion objectives should be compared. First, both types of objectives permit high NA imaging. Secondly, water and oil immersion objectives are the most common immersion objectives in use today. For our study, two samples are examined: (1) autofluorescent human skin, and (2) sulforhodamine B (model drug) treated skin.

MATERIALS AND METHODS

The multi-photon microscope used in this study has been well described in the literature (So et. al., 2000). An instrument diagram of our set up is shown in Fig. 1. The excitation source is an argon-ion (Innova 300, Coherent, Santa Clara, CA) pumped, femtosecond titanium-sapphire laser (Mira 900, Coherent). Output of the titanium-sapphire (Ti-Sa) laser beam is directed toward an x-y scanning system (Model 6350, Cambridge Technology, Cambridge, MA) that reflects the Ti-Sa laser, at different angles, into the microscope (Zeiss Axiovert 100 TV, Thornwood, NY). At the entrance of the microscope, the laser is beam expanded by a lens combination to ensure overfilling of the objective's back aperture. The expanded beam is then reflected into the objective by a dichroic mirror. Either the well-corrected, high NA, water-immersion objective (Zeiss, 40× C-Apochromat, NA 1.2) or the high NA oil-immersion objective (Zeiss, 40× Fluar, NA 1.25) was used for imaging. The fluorescence generated at the focal spot is collected by the objective, transmitted through the dichroic mirror and optical filters before being recorded by the photomultiplier tube (PMT). In our single-photon counting, detection scheme, the signal from the PMT is processed by a discriminator before recorded by the computer. The fluorescence image of the specimen is constructed by recording the fluorescent photons at each pixel imaged.

Three-dimensional (3-D) scanning of the sample is achieved by a combination of the galvo-driven, x-y scanning mirrors of the beam and axial positioning of the objective's focal spot. Axial positioning of the objective was achieved by a piezo-driven objective stage (P-721 PIFOC®, Physik Instrumente (PI), Germany)

which can provide a full axial scanning range of 72.4 μm. The 3-D image stack acquired in this manner is composed of axial image frames with a typical separation of 0.724 μm. Each image frame is composed of 256 × 256 pixels, with a pixel separation of 0.242 μm. For axial scanning beyond the range allowed by the piezo-driven, objective stage, the manual objective focus control is used with the piezo stage to achieve the desired imaging depth.

Two types of skin samples were imaged using the two objectives. First, the skin used for imaging of autofluorescence is prepared by placing a piece of excised human skin (in the mm size range) in the center of a rubber gasket. A coverglass is placed on the adhesive side of the gasket to seal the sample, and a small piece of damp tissue is sandwiched between the back side of the skin and the glass slide to ensure solid contact between the skin and the coverglass. The damp tissue also helps to keep the skin moist during image acquisition. The second skin specimen we imaged was sulforhodamine B–treated, human skin sample. This system is of interest because similar systems have been used to study the drug delivery mechanism in which sulforhodamine B molecules was used as the model drug. Specifically, the influence of the chemical enhancer oleic acid on the penetration profiles of hydrophilic sulforhodamine B was compared to that of hydrophobic rhodamine B hexyl ester, RBHE (Yu et. al., 2001). In this study, we use the sulforhodamine B containing skin sample for comparing the rhodamine B fluorescence profiles obtained using both objectives. The preparation of the sulforhodamine B containing skin samples is similar to the protocol listed in a previous work (Yu et al., 2001). In this procedure, human cadaver skin from the abdominal area (National Disease Research Interchange, Philadelphia, PA), obtained 10–20 hours post-mortem, was used. The skin specimens were stored at −80°C and used within 3–6 weeks. For the model drug delivery studies, the skin was first thawed at room temperature of 25°C, and the dermal fat was removed. The skin samples 2.25 cm^2 in area were mounted in side-by-side diffusion cells (9-mm diameter, PermeGear, Riegelsville, PA). Donor vehicle solution was of sulforhodamine B in a 1:1 volume mixture of ethanol (100%, Pharmco™ Products, Brookfield, CT) and PBS (Sigma, St. Louis, MO). The skin samples remained in contact with the donor solution for 24 hours. Prior and after the skin exposure to the donor solution, skin conductivity measurements were conducted in phosphate buffered saline, PBS (0.01 M phosphate buffer, 0.0027M KCl and 0.137 M NaCl, pH = 7.4, Sigma). To prepare the skin specimens for multi-photon imaging, the samples were rinsed with the 1:1 PBS-ethanol solution and blotted with Kimwipe (Kimberly-Clark®, Roswell, GA) to remove excess fluorescent probes from the skin surfaces. The circular region of the skin specimens exposed to the donor solution was then excised with a surgical carbon steel razor blade (VWR Scientific, Media, PA) and sealed in an imaging chamber (2.5 mm Coverwell™, Grace Bio-Labs, Bend, OR) with a cover slip in contact with the stratum corneum side. A drop of PBS was added to the chamber to maintain the moisture with the imaging chamber.

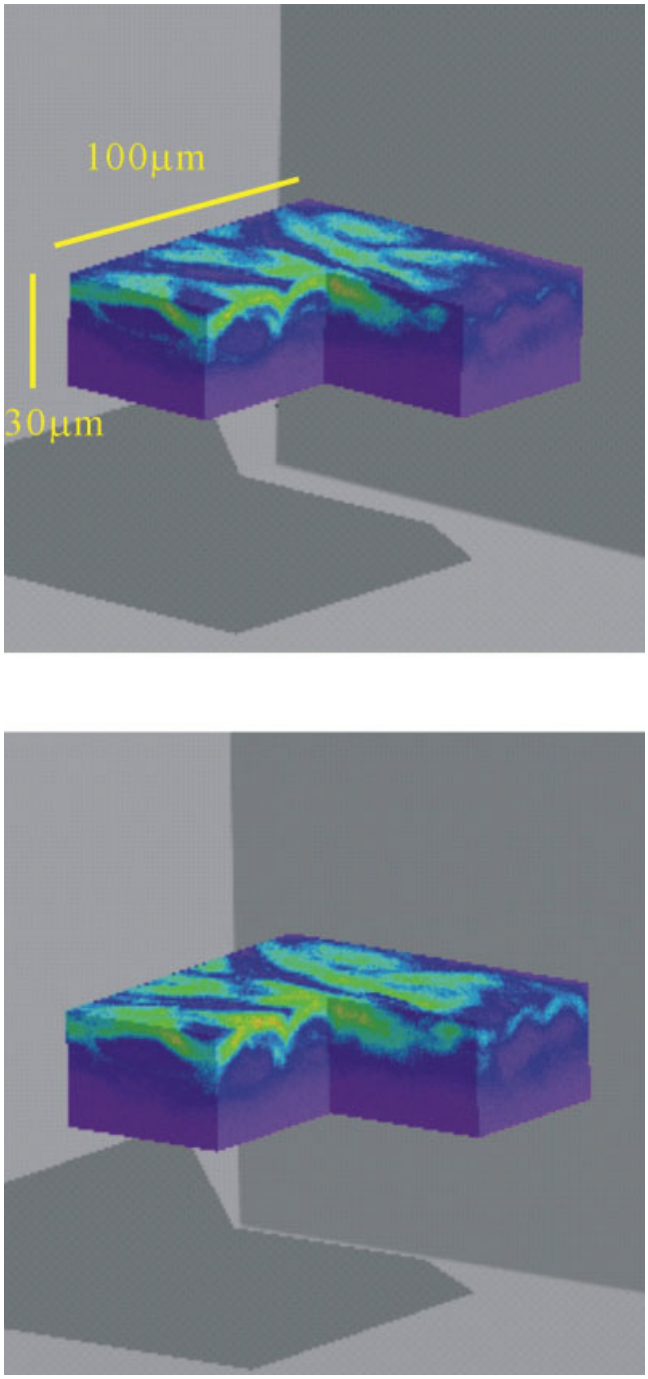

Fig. 4. Three-dimensional image stack of sulforhodamine B treated skin taken using the water (**top**) and oil (**bottom**) immersion objectives.

The comparison of the performance between the two objectives is based on two criteria. In the case of skin imaging, images acquired using the water and oil immersion objectives at different depths are placed side-by-side and judged for image quality. While image appearance can be indicative when the two immersion objectives perform visibly different, such comparison

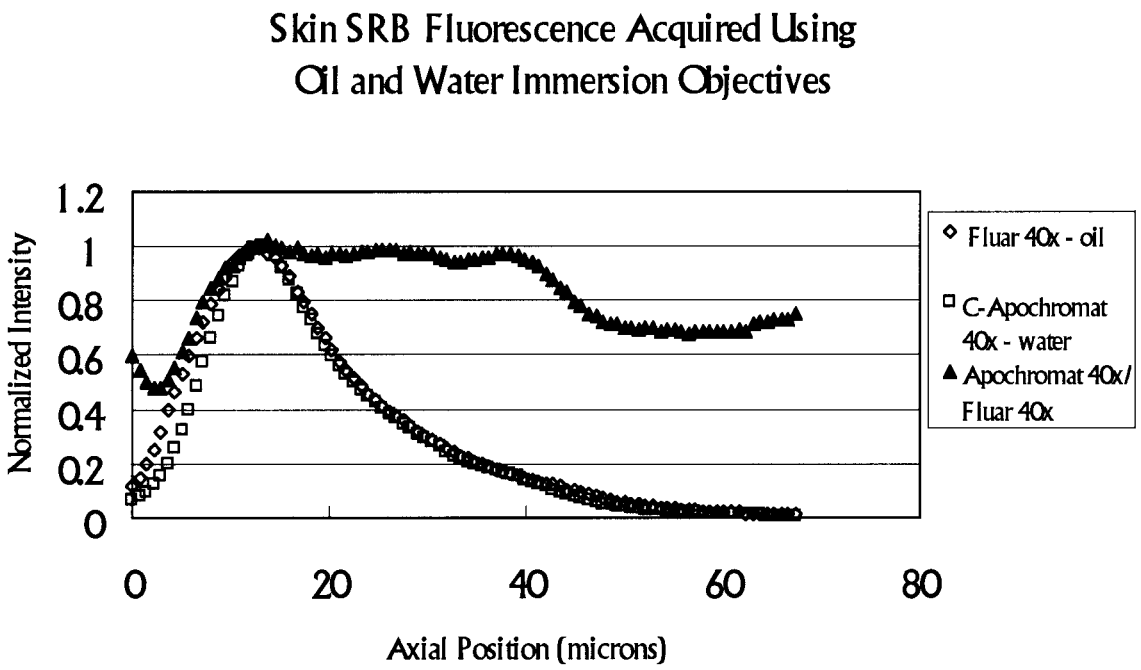

Fig. 5. Sulforhodamine B axial profiles (with fluorescence ratio) in skin recorded with the water and oil immersion objectives.

does not reveal subtle difference in point-spread-function. Therefore, the two objectives are compared by the measured intensity profile at each focal plane.

RESULTS AND DISCUSSION

Axial Fluorescence Intensity Distribution

The measured axial fluorescence intensity profiles using the water and oil immersion objectives are calculated in the following manner. At each axial position, the fluorescence intensity of the image frame is averaged. Next, the axial profile is obtained by plotting the average intensity of each frame at different axial positions.

While the optical properties of uniform, aqueous fluorescence solutions can be well controlled and the choice of water immersion objective in imaging this type of specimens clear, it is difficult to draw similar conclusions for imaging an optically heterogeneous specimen such as the human skin. In this case, we compared the multiphoton image quality and axial fluorescence profiles acquired using the water and oil immersion objectives. To compare the images, autofluorescence images from nearby layers in the stratum corneum, deeper epidermis, basal layer, and upper dermis were selected from the 3-D image stack. For the comparison between the two objectives, image frames are selected and placed side-by-side for analysis. These results are shown in Figure 2. In addition, axial auto-fluorescence intensity profiles acquired with the type objectives are also calculated and plotted in Figure 3. Moreover, the ratios of the intensity acquired from the two objectives were calculated and plotted in the same figure. In this case, the fluorescence intensity ratio was calculated as the ratio between the C-Apochromat 40× objective intensity to that acquired with the Fluar 40× lens. For an accurate comparison, the same region of the skin was imaged. Examination of Figure 2 shows that skin auto-fluorescence images acquired with the two objectives matches closely in appearance. This observation appears to support the fact that both objectives perform comparably in the skin. This apparent conclusion is supported by a casual examination of the auto-fluorescence depth profiles shown in Figure 3. Up to depths > 65 μm, the two objective profiles match each other closely. However, an examination of the intensity ratio between the two objectives reveals a different story. Up to the axial position of approximately 60 μm, the intensity ratio between the two objectives fluctuates about 1, indicating that the water and oil lens PSF's are comparable in that region. However, beyond 60 μm, the intensity ratio starts to drop steadily to below 1. At the deepest imaging depth, the ratio drops to below 0.9, indicating that the water immersion objective detects approximately 10% less signal than the oil lens.

In addition to the autofluroescent skin, skin specimens treated with sulforhodamine B were also imaged and compared with the water and oil immersion objectives. The multi-photon 3-D image stacks are shown in Figure 4, and the corresponding fluorescence profiles are calculated and displayed in Figure 5. As in the case for autofluorescent skin, the intensity ratio between the water and oil lenses was calculated and plotted. Visual examinations of Figures 4 and 5 shows that the 3-D image stacks acquired using both objectives display similar image quality. The axial cross-sectional views show no evidence in objective dependent image degradation. In addition, the two sulforhodamine B profiles of Figure 5 agree well with each other. However, the ratio plot reveals that beyond the depth of

approximately 40 μm, the intensity ratio steadily decreases. In the axial region between 40 μm and the deepest imaging depths, most of the intensity ratios fluctuate between 0.7 and 0.8, indicating that at the greater imaging depths, the oil immersion objective is more efficient in generating and collecting the SRB fluorescence by more than 30%.

In the case of autofluorescent skin, the ratio decay point (at about 60 μm) corresponds to the basal layer of the sample we imaged. Therefore, the autofluorescence results indicate that although the skin refractive index varies from 1.47 to 1.34 in the epidermis. The differential effects of spherical aberration between the two objectives are not apparent until the dermis is reach (refractive index of 1.41) (Knüttel and Boehlau-Godau, 2000; Tearney et al., 1995). Beyond the epidermal-dermal junction, the oil immersion objective outperforms the water objective by about 10% in the fluorescence generation and detection efficiency. In the case of SRB-treated skin, the detection of the SRB fluorescence prevents an autofluorescence determination of the physical barrier (at 40 μm) responsible for the intensity ratio decay at 40 μm. However, the autofluorescence skin results will support the 40-μm position as the point of the epidermal-dermal barrier.

Nonetheless, in the case of the SRB skin sample, the water and oil immersion objectives perform comparably at the initial layers of the skin. Beyond the epidermal-dermal junction, the oil objective is capable of generating and collecting fluorescence more efficiently than the water objective.

CONCLUSIONS

While the effects of scattering and spherical aberration on microscopic image formation in optically homogenous samples are well documented, the difference in performance between objectives of different immersion fluids in thick, optically complex specimen such as the human skin remains unclear. While the exact characterization of imaging parameters inside the skin is difficult, we addressed this issue by analyzing and comparing the multi-photon skin images acquired using oil and water immersion objectives. The results from our study demonstrate the important result that the water and oil objectives perform comparably in surface skin layers up to the epidermal-dermal junction. Beyond the junction, the oil lens is more efficient in generating and collecting multi-photon fluorescence, by as much as 30%. This effect is most likely due to the fact that the stratum corneum has a refractive index more closely matched to that of the immersion oil and, therefore, the oil objective would experience lesser effects of spherical aberration when imaging deep within the skin. In conclusion, provided that the working distance is adequate, an oil immersion objective should be used over a comparable water lens in multi-photon skin imaging applications.

REFERENCES

Centonze VE, White, JG. 1998. Multiphoton excitation provides optical sections from deeper with scattering specimens than confocal imaging. Biophys J 75:2015–2024.

de Grauw CJ, Vroom JM, van der Voort HTM, Gerritsen, HC. 1999. Imaging properties of two-photon excitation microscopy and effects of refractive-index mismatch in thick specimens. Appl Optics 38: 5995–6003.

Denk W, Strickler JH, Webb WW. 1990. Two-photon laser scanning fluorescence microscopy. Science 248:73–76.

Dong CY, Koenig K, So PTC. 2003. Characterizing point spread functions of two-photon fluorescence microscopy in turbid medium. J Biomed Optics 8:450–459.

Dunn AK, Wallace VP, Coleno M, Berns MW, Tromberg BJ. 2000. Influence of optical properties on two-photon fluorescence imaging in turbid samples. Appl Optics 39:1194–1201.

Gerritsen HC, de Grauw CJ. 1999. Imaging of optically thick specimen using two-photon excitation microscopy. Microsc Res Tech 47:206–209.

Halliday D, Resnick R, Krane KS. 1992. Physics, vol. 2. New York: John Wiley & Sons, Inc.

Hell S, Reiner G, Cremer C, Stelzer EHK. 1993. Aberrations in confocal fluorescence microscopy induced by mismatches in refractive index. J Microsc 169:391–405.

Knüttel A, Boehlau-Godau M. 2000. Spatially confined and temporally resolved refractive index and scattering evaluation in human skin performed with optical coherence tomography. J Biomed Optics 5:83–92.

Masters BR, So PTC, Gratton E. 1997. Multiphoton excitation fluorescence microscopy and spectroscopy of in vivo human skin. Biophys J 72:2405–2412.

Piston DW, Masters BR, Webb WW. 1995. Three-dimensionally resolved NAD(P)H cellular metabolic redox imaging of the in situ cornea with two-photon excitation laser scanning microscopy. J Microsc 178:20–27.

So PTC, Dong CY, Masters BR, Berland KM. 2000. Two-photon excitation fluorescence microscopy. In: Annual Review of Biomedical Engineering, vol. 2. Annual Reviews, Palo Alto, p 399–429.

Squirrell JM, Wokosin DL, White JG, Bavister BD. 1999. Long-term two-photon fluorescence imaging of mammalian embryos without compromising viability. Nat Biotechnol 17:763–767.

Svoboda K, Denk W, Kleinfeld D, Tank DW. 1997. In vivo dendritic calcium dnamics in neocortical pyramidal neurons. Nature 385: 161–165.

Tearney GJ, Brezinski ME, Southern JF, Bouma BE, Hee MR, Fujimoto JG. 1995. Determination of the refractive index of highly scattering human tissue by optical coherence tomography. Optics Lett 20:2258–2260.

Yu B, Dong CY, So PTC, Blankschtein D, Langer R. 2001. In vitro visualization and quantification of oleic acid induced changes in transdermal transport using two-photon fluorescence microscopy. J Invest Dermatol 117:16–25.

Yu B, Kim KH, So PTC, Blankschtein D, Langer R. 2002. Topographic heterogeneity in transdermal transport revealed by high-speed two-photon microscopy: determination of representative sample sizes. J Invest Dermatol 118:1085–1088.

Yuste R, Denk W. 1995. Dendritic spines as basic functional units of neuronal integration. Nature 375:682–684.